PHYSICAL REVIEW A VOLUME 22, NUMBER 5 NOVEMBER 1980

Single- and double-electron loss from helium by collisions with $v \geq v_0$ multiply charged ions

P. Hvelplund, H. K. Haugen, and H. Knudsen
Institute of Physics, University of Aarhus, DK-8000 Aarhus C, Denmark
(Received 12 May 1980)

Cross sections for single- and double-electron loss (electron capture plus impact ionization) for H^+, He^{q+}, O^{q+}, and Au^{q+} incident on helium have been measured at velocities from $\sim v_0$ to $\sim 10v_0$. The charge state q was varied from 1 to 21, depending on velocity and projectile. The energy and charge-state dependence of the single-loss cross section at the lower velocities is reasonably well described by the model of Olson based on Coulomb interaction between particles and classical trajectory Monte Carlo calculations. The results for H^+, He^+, and He^{++} at high velocities are in good agreement with earlier experimental values of Pivovar *et al.* and with Bethe-Born calculations of Gillespie. The double-loss cross section, which for highly charged projectiles amounts to as much as 60% of the single loss, is found to behave quite differently from the single-loss cross section, both as a function of incident charge and velocity. While single-loss cross sections at velocities between v_0 and $2v_0$ are almost independent of energy and proportional to q, the double-loss cross sections are approximately proportional to energy and to q^2.

I. INTRODUCTION

Collisions between multicharged ions and atoms is a research area which has experienced its renaissance in connection with the controlled thermonuclear-fusion development programme (see, e.g., Gilbody,[1] de Heer,[2] Olson,[3] and Salzborn and Müller).[4] This research area had earlier been of interest because of its importance in connection with the slowing down of fission products in matter, and theoretical papers on this subject have been published by Bohr,[5] Bell,[6] and Bohr and Lindhard,[7] while experimental investigations have been performed by Lassen[8] and others. Later, along with the development of accelerators and ion sources, a great deal of experimental investigations with highly charged ions were performed (for reference, see, e.g., Betz[9]).

The aim of the present investigation is to make a broad experimental survey of electron loss by a simple atom (helium) in collisions with multicharged ions at velocities comparable with the velocity of the active electrons. Accordingly, the interaction can, to a first approximation, be thought of as a Coulomb interaction between a point charge and a two-electron atom. Helium is chosen as the target because it is the simplest atom which can be used in a standard target cell and because investigations of helium can be partly understood by applying the formalism developed in connection with the highly charged-ion interaction with atomic hydrogen by, e.g., Duman *et al.*,[10] Janev and Presnyakov,[11] Olson and Salop,[12] and Ryufuku and Watanabe,[13] and further can give information related to interaction with multielectron systems.

The processes investigated here can be expressed in the form

$$X^{q+} + \mathrm{He} \rightarrow \begin{cases} X^{(q+l)+} + \mathrm{He}^+ + (l+1)e, & [\sigma(1)] \\ & Z-q \geq l \geq -1 \\ X^{(q+l)} + \mathrm{He}^{++} + (l+2)e, & [\sigma(2)] \\ & Z-q \geq l \geq -2\ . \end{cases} \quad (1)$$

$\sigma(1)$ is the total cross section for loss of one electron from the target atom and $\sigma(2)$ is the total cross section for loss of two electrons. In the experiments reported here, the largest contributions to the cross sections are stemming from processes with $l=-2$, -1, and 0, but more detailed experiments are needed in order to be more specific with regard to the relative importance of processes associated with those l values.

Measurements are reported for H^+, He^+, and He^{++} at energies from 0.5–5 MeV/amu, for 125-keV/amu O^{q+} ($q=1,\ldots,6$), 1-MeV/amu O^{q+} ($q=3,\ldots,8$), 16.8-keV/amu Au^{q+} ($q=1,\ldots,8$), 60-keV/amu Au^{q+} ($q=3,\ldots,17$), and 100-keV/amu Au^{q+} ($q=5,\ldots,21$). The cross sections were measured by a time-of-flight spectrometer, see, e.g., Cocke,[14] and put on an absolute scale via condenser-plate measurements where the slow ions are collected. The results are discussed in connection with existing theoretical models with special emphasis on scaling laws.

II. EXPERIMENTAL TECHNIQUE

A. Apparatus

Figure 1 shows schematically the experimental arrangement used for the present measurements. A continuous or pulsed beam of monoenergetic ions in a preselected charge state was provided by an EN tandem accelerator equipped with a 90° analyzing magnet. A post-stripper foil installed

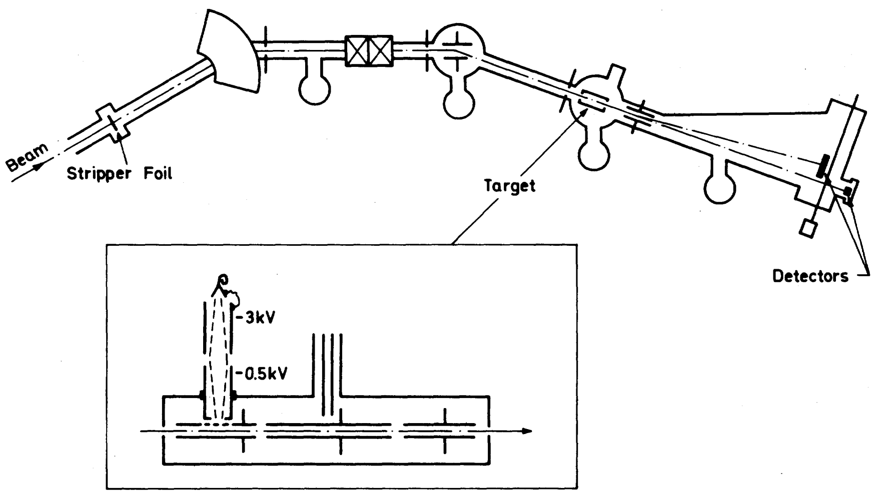

FIG. 1. Schematic diagram of the apparatus discussed in Sec. II.

between this magnet and the switching magnet converted the mono-charge-state beam into a beam containing a broad distribution of charge states, depending on ion type and energy. Subsequent magnetic analysis allowed the selection of the desired incident-charge state.

After the switching magnet, the beam passed an ~8-m long beam tube provided with a quadrupole for focusing. Approximately 1 m before the target chamber, the beam was cleaned for unwanted charge states by a set of electrostatic deflection plates. From this point on, the rest-gas pressure was $\sim 5\times 10^{-7}$ Torr. After passing an adjustable aperture of 0.5×0.5 mm^2, the beam entered the gas cell through a 1-mm diameter aperture and emerged through a 3-mm diameter aperture. Finally, the beam intensity was measured by a detector, which was either a negatively biased Faraday cup, a channel-electron multiplier, or a solid-state detector. The extra set of electrostatic deflection plates shown in Fig. 1 was used for charge dispersion in connection with a solid-state, position-sensitive detector when electron capture was measured (see a forthcoming article).

The gas-handling system for the target consisted of a stainless-steel reservoir equipped with a remote-controlled needle valve and a Pirani gauge, which has been calibrated against a membrane manometer on a separate setup. The pressure in the reservoir was kept above atmospheric pressure, and the reservoir was refilled between each run. The helium-target gas used was at least 99.99% pure, and target impurities are believed not to affect the cross-section values.

The insert in Fig. 1 shows the target cell, which consists of a 22-cm long, 5-cm diameter tube with entrance and exit apertures as stated above and is equipped with 10-cm long condenser plates. Guard plates were used to provide a uniform electric field in the collision region. The guard plate in the upstream end of the gas cell further served as the first electrode in a time-of-flight spectrometer. A hole in the guard plate is covered by a nickel mesh with a transparency of 64%. The second electrode in the spectrometer is a 4-cm long, 2-cm diameter tube with a 3×5-mm^2 entrance slit. The third electrode is a 4-cm long, 2-cm diameter tube separated approximately 1 cm from the second electrode. The detector is a channel-electron multiplier. The dimensions of the spectrometer are determined partly by the requirements to time resolution and partly by beam-optics considerations.

B. Condenser measurements

The condenser measurements were performed with the direct beam or with the most intense charge-state components of the beam transmitted through the carbon foils. Slow ions produced by the interaction between projectiles and target atoms were collected on the condenser plates by applying a transverse electric field to the target region. This electric field was increased until the collected current reached a saturation value (40 V/cm). To estimate the current caused by secondary emission from the surface of the negative plate, a magnetic field was supplied to the target region. By increasing the field strength up to a point (~150 Oe) where no further current changes were observed, we found that our measurements with no magnetic field had to be corrected by 15%. This value is in reasonable agreement with the experimental data (of Kaminsky[15]) for potential emission caused by low-energy He^+ particles impinging on a "dirty" aluminum surface. For a general discussion of the condenser method, see, e.g., Massey and Gilbody.[16]

The loss cross sections were determined by measuring simultaneously the slow ion current to the condenser plate and the beam current to the Faraday cup. Measurements were performed at different velocities, and the cross section was determined from the expression

$$\sigma_t = \lim_{p \to 0}\left(\frac{I - I_0}{p I_b}\right) q \Big/ (l \times 3.29 \times 10^{16}), \qquad (2)$$

where I is the slow ion current, I_0 is the same current due to rest gas, and I_b is the beam current. p is the pressure in Torr (normally $\sim 10^{-3}$ Torr), l is the target length in cm, and σ_t is in cm^2. The measured cross section σ_t is related to the cross section for single loss $\sigma(1)$ and for double loss $\sigma(2)$ by

$$\sigma_t = \sigma(1) + 2\sigma(2). \qquad (3)$$

Clearly, the condenser measurements alone give no information on the relative size of $\sigma(1)$ and $\sigma(2)$. The overall uncertainty in these cross sections is estimated to be $\pm 10\%$.

C. Time-of-flight measurements

During the time-of-flight measurements, the beam intensity was drastically reduced; it was monitored either by a channel-electron multiplier or a solid-state detector with a typical count rate of 3000 counts/s. The tandem accelerator was operated in a pulsed mode with a pulse repetition period of 1 μs and a pulse width of 10 ns. Pulses from the time-of-flight spectrometer channeltron generated a fast signal, which was used to start a time-to-amplitude converter. The stop pulses were generated by the master clock of the pulsing system.

The potential of the collector plates was ± 0.4 kV, the potential of the second electrode -0.5 kV, and that of the third electrode and the funnel -3 kV. These are the design values of the spectrometer, and it was found that its efficiency did not change with moderate variations in these potentials. It should be noted here that beam deflection in the target cell was eliminated by switching the polarity on the condenser plates since these are twice as long as the guard plates.

A typical time-of-flight spectrum is shown in Fig. 2. As the only information of interest in the present connection is the content of the two peaks, it is easily seen that the resolution is excellent and that background can be corrected for when necessary with no difficulty. The time interval between two peaks is ~ 200 ns.

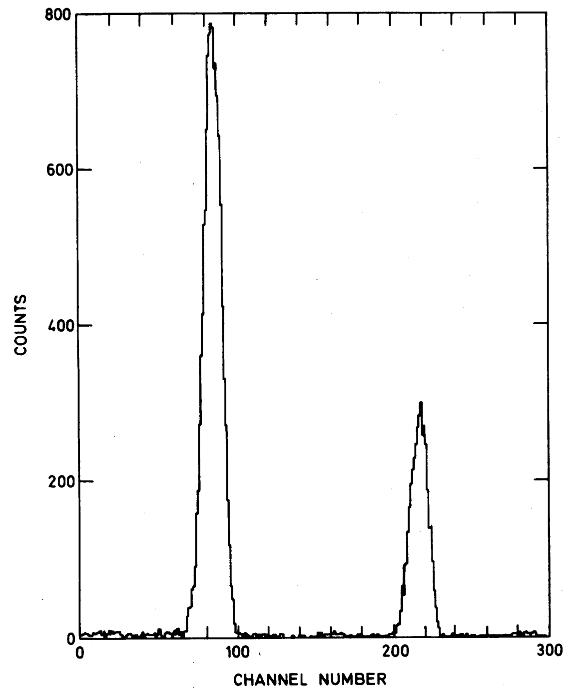

FIG. 2. Time-of-flight spectrum for He ions produced by impact of 125-keV/amu O^{6+}. The larger peak corresponds to He^+ ions and the smaller one to He^{++} ions. Target pressure: 2.32×10^{-3} Torr.

In an actual measurement, time-of-flight spectra were recorded at various pressures for a given number of counts registered by the projectile counter. From such measurements, two quantities were determined, viz., $\lim_{p\to 0} F(1)/p$ and $\lim_{p \to 0} F(2)/p$, where $F(1)$ and $F(2)$ are the number of counts in the He^+ and He^{++} peak divided by the number of recorded projectiles, respectively. Denoting the ratios of these two quantities by f, we obtain

$$f = \frac{\sigma(2)}{\sigma(1)} = \lim_{p \to 0} \frac{F(2)}{p} \Big/ \lim_{p \to 0} \frac{F(1)}{p}, \qquad (4)$$

since $\lim_{p \to 0} F/p$ is proportional to σ. The single- and double-loss cross sections were determined from the relations

$$\begin{aligned} \sigma(1) &= \sigma_t/(1+2f), \\ \sigma(2) &= f\sigma_t/(1+2f), \end{aligned} \qquad (5)$$

in the cases where we have condenser-plate measurements as well. The efficiency of the time-of-flight spectrometer was found not to depend on the charge state of the incoming ion. In the case of 20-MeV gold, we measured with both the condenser plates and the time-of-flight spectrometer for incoming charge states of 5, 13, 14, 15, and 16 and found that the efficiency is constant within 10%. Since the relative intensity of singly and doubly charged helium ions changes by approximately 30% by going from $q=5$ to $q=16$, this observation also supports the assumption that the efficiency of the time-of-flight spectrometer is close to being independent of the charge state of the collected ions. This assumption is furthermore supported by similar measurements by Cocke.[14] The most likely reason for a possible difference in the collection efficiency of He^+ and He^{++} would be differences in channeltron efficiency for 3-keV He^+ ions compared with 6-keV He^{++} ions. Measurements by Burrous *et al.*[17] indicate that a 5–10% discrepancy might be expected, with He^{++} being counted with the highest efficiency.

By assuming a target length of 0.5 cm, the geometrical length of the slit, we find that the overall efficiency of the time-of-flight spectrometer is ~40%. Here it should be borne in mind that the grid transmission is ~60% and that the channeltron efficiency is probably slightly smaller than one.

Figure 3 shows plots of $F(1)/p$ and $F(2)/p$ as functions of p for 2-MeV O^{q+} ions incident on helium. In this case, the cross sections for $q=2$ are put on an absolute scale by comparing with condenser measurements, and since $\lim_{p\to 0} F/p$ is proportional to cross sections, absolute cross sections are obtained for all incident-charge states.

It should here be emphasized that by combining time-of-flight measurements with condenser measurements, two advantages are obtained. First, we can measure the individual cross sections, $\sigma(1)$ and $\sigma(2)$, and not only σ_t. Second, measurements over a much broader charge-state range can be performed since beams with intensities down to 10^{-16} A can be used.

When using helium and hydrogen as projectiles, we found by comparison to a solid-state detector that the efficiency of the beam channeltron was smaller than one and that it depended on the charge state of the incoming ion. Therefore, instead of the channeltron, for these projectiles we used the solid-state detector, which has an efficiency of one for all charge states. (By comparing the intensity measured with the channeltron and that measured with the solid-state detector, we found that at 8 MeV, the channeltron had an efficiency of 56% for He^+ and 77% for He^{++}. This effect is due to the low secondary-electron-emission coefficient for high-velocity particles in connection with small charge-changing cross sections in the solid surface of the detector.)

The estimated error on our absolute cross sections is approximately 15%, while the relative uncertainties in a single run, where only the charge state is varied, is only a couple of percent.

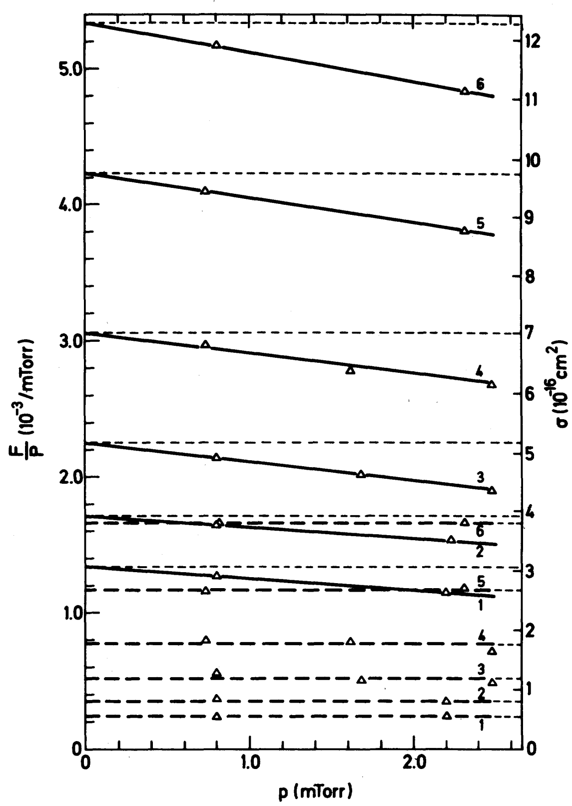

FIG. 3. Experimental time-of-flight results (cf. text) for 2-MeV O ions. Solid lines through the experimental points represent a linear extrapolation to zero of $F(1)/p$ vs p. Similarly, dashed lines represent $F(2)/p$ vs p. The charge state of the incident ion is indicated on each curve. Experimental values of $\lim_{p\to 0}F/p$ are brought on an absolute scale, shown in the right-hand side of the figure, via condenser measurements, in this case for O^{2+} ions.

III. RESULTS AND DISCUSSION

A. Theoretical background

The most important interaction when a highly charged particle passes by an atom is the Coulomb attraction between the projectile and the target electrons. This interaction may cause a transition from the initially bound target state to a final continuum state or bound projectile state. In order to bring out the principal arguments as clearly as possible, we will consider the problem assuming classical mechanics to be applicable. This assumption is well justified since the Bohr[5] parameter $\kappa=2qv_0/v$ is much larger than one for most cases treated in this paper. Ionization was originally treated by Thomson.[18] He assumed that the velocities of target electrons are small compared to the projectile velocity and that the projectile interacts only with one target electron and, further, that its nucleus provides only the binding energy and is otherwise not considered. Ionization is supposed to happen when a collision with an energy transfer T larger than the binding energy I has taken place. The differential cross section for collisions between a free electron at rest and a projectile with charge q and velocity v is given by

$$d\sigma = (2\pi q^2 e^4/mv^2)dT/T^2, \tag{6}$$

where e and m are the electron charge and mass, respectively.

By integrating Eq. (6) from the binding energy I to the maximum energy transfer $2mv^2$, one obtains for the total ionization cross section

$$\sigma = 4\pi a_0^2 q^2 (v_0/v)^2 I_0 (1/I - 1/2mv^2), \tag{7}$$

where $a_0 = \hbar^2/me^2$, $v_0 = e^2/\hbar$, and $I_0 = \frac{1}{2}mv_0^2$. If we further make the assumption that $I \ll 2mv^2$, the ionization cross section takes on the form

$$\sigma = 4\pi a_0^2 q^2 (v_0/v)^2 I_0/I. \tag{8}$$

This formula shows the well known q^2 and $1/E$ dependence of the ionization cross section at high energies.

Following Bohr's[5] argument, the atomic-binding forces introduce a dynamic screening. Encounters of time durations long compared to the atomic period will be adiabatic in character, and the electron will not be ejected in such collisions. As Bohr points out, the usual definition of the adiabatic distance does not apply for highly charged projectiles interacting with loosely bound electrons, since during the collision the binding of the electron may be disrupted.

Let us follow Bohr's notation and call the limiting value of the impact parameter, for which the probability of ionization is still of the order of unity, d^*. This impact parameter is found by setting the work performed on the electron under consideration during one revolution equal to its binding energy. We thus obtain

$$(qe^2/d^{*2})2a = I, \tag{9}$$

where a is the radius of the electron orbit. The energy transfer to a free electron at this impact parameter is

$$T_1 = q(v_0/v)^2 I_0 (I/I_0)^{3/2}. \tag{10}$$

Replacing I in Eq. (8) by T_1, we obtain

$$\sigma = 4\pi a_0^2 q (I_0/I)^{3/2}, \tag{11}$$

valid for $T_1 > I$ or E (keV/amu)$/q < 25(I/I_0)^{1/2}$. We notice that because of dynamical screening, the ionization cross section becomes independent of energy and linearly dependent on q. As seen from Eq. (7), collisional ionization eventually decreases because it is no longer possible to transfer an energy larger than the binding energy to the electron.

For a simple description of the capture part of the loss cross section, we shall follow the treatment given by Bohr and Lindhard.[7] They defined the release distance R as the distance between the highly charged projectile and the target atom, at which the force on the electron from the projectile and that from the target nucleus are approximately equal. This gives

$$qe^2/R^2 = mu^2/a, \tag{12}$$

where we assume the electron in question to have an orbital velocity u.

The condition for capture is that the release takes place where the total energy of the electron relative to the ion has a negative value, i.e., within a distance R' given by

$$qe^2/R' \simeq \tfrac{1}{2}mv. \tag{13}$$

If $R < R'$, capture occurs with a cross section

$$\sigma_c \simeq \pi R^2 = \pi a_0^2 q (I_0/I)^2, \tag{14}$$

whereas, if $R' < R$, a more elaborate analysis gives

$$\sigma_c = \pi a_0^2 q^3 (I/I_0)(v_0/v)^7. \tag{15}$$

It should be pointed out that the cross section at low velocity and high charge states varies as q, while at high velocities, the cross section increases as q^3 and decreases strongly with velocity.

In Fig. 4 the energy dependence of the various cross sections for X^{20+} on He is shown. At low velocities, the total loss cross section is dominated by electron capture and at higher velocities by ionization. In the energy-independent region,

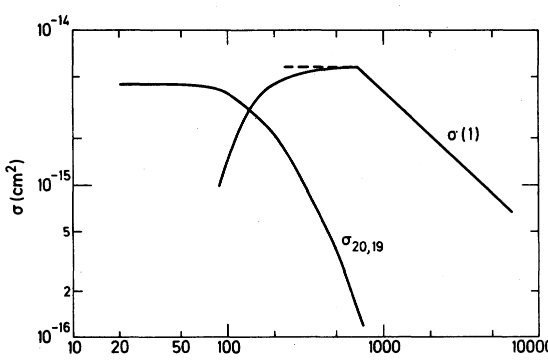

FIG. 4. Cross sections for single ionization $\sigma(1)$ and single capture $\sigma_{20,19}$ by a twenty-times charged projectile incident on He. The ionization is found from Eqs. (7), (8), and (11). Dashed line corresponds to Eq. (8), which is a high-energy approximation within its range of validity. The capture cross sections are found from Eqs. (14) and (15) but with a more realistic electron distribution (see forthcoming article).

the loss cross section is proportional to q; at high energies, it is proportional to q^2. It should also be borne in mind that at lower q values, where capture will not always compensate for the decrease in ionization, the loss cross sections will decrease for decreasing energy.

In the region where both electron capture and ionization are important, a classical Monte Carlo method has been used by Olson.[19] In this approach, the cross sections were estimated by solving Hamilton's equation of motion for a three-body system numerically. The three bodies were the incident ion, the helium-ion target, and the electron initially moving around the helium ion. The interaction between the three bodies is Coulombic. After completion of the interaction, it is determined whether the active electron is still on the target (no reaction), bound to the projectile (electron capture), or free (ionization). The classical Monte Carlo method was first applied successfully to a one-electron target[20] (hydrogen), and an extension to multielectron targets is not straightforward. Olson[19] used the results for one-electron systems as far as possible but introduced effective charge and correlation factors in order to calculate the loss cross section for helium atoms. As was shown also for one-electron targets, Olson found that the total single-electron-loss cross section divided by the projectile charge falls on a single curve when plotted versus collision energy in keV/amu divided by the charge state. This type of reduced plot is a convenient way of plotting single-electron-loss cross sections, and its applicability and limitations are discussed in the next section.

To the best of our knowledge, there exists no treatment of double loss for projectile velocities of the order of the electron velocities in the atom, where a binary-encounter approximation cannot be applied. At higher velocities where such an approximation can be applied, both Olson[21] and Cocke[14] have estimated the double-loss cross section. Olson applied the so-called independent-electron model. In this model, the multiple-ionization-transition probabilities $P_n(b)$ for removing n electrons from a shell containing N electrons, in a collision with impact parameter b, are given by

$$P_n(b) = \binom{N}{n} P_s(b)^n [1 - P_s(b)]^{N-n} , \qquad (16)$$

where $\binom{N}{n}$ is the binomial coefficient and $P_s(b)$ is the transition probability calculated by the classical Monte Carlo method in a one-electron model, where an appropriate binding energy is chosen. Cocke[14] treated the double-electron loss in what is called the energy-deposition model, where the electrons are first excited and then ejected. A detailed discussion of these treatments will not be given here since they apply to very few of the experimental results reported in the present paper.

Returning now to single-electron loss at high energies, the classical description becomes invalid, and a quantal treatment must be applied, viz., the Born or the Bethe-Born approximation. In this approximation, the ionization cross section can be written in the form (Gillespie[22])

$$\sigma = 4\pi a_0^2 \frac{\alpha^2}{\beta^2}\left[q^2 M_{\text{ion}}^2\left(\ln\frac{\beta^2}{1-\beta^2} - \beta^2\right) + C_{\text{el, ion}} + 2I_{\text{in, ion}} + (\gamma_{\text{el, ion}} + 2\gamma_{\text{in, ion}})\frac{\alpha^2}{\beta^2}\right]. \qquad (17)$$

Here, $\beta = v/c$, α is the fine-structure constant, and M_{ion} is the total dipole-matrix element for ionization of the target atom.[23] The parameters $C_{\text{el, ion}}$, $\gamma_{\text{el, ion}}$, $I_{\text{in, ion}}$, and $\gamma_{\text{in, ion}}$ involve properties of both the ion and the atom. Numerical values for these parameters have been calculated by Gillespie.[22] It should be noted that the cross sections vary as $\ln E/E$ and for bare nuclei are proportional to q^2. For projectiles carrying electrons such as He^+, a significant deviation from a q^2 scaling is found. A similar effect has been found by Bell *et al.*[24] by applying Born-approximation calculations for He^+ projectiles in helium. By comparing these calculations with calculations by Bell and Kingston[25] for proton-ionization cross sections, they found that in the energy range from 0.1 to 4 MeV, the ionization cross section of helium by He^+ ions may be obtained from the cross sections of ionization of helium by protons by applying a q^2 relationship but introducing an effective q, which for He^+ is 1.25. This value is only slightly energy dependent.

B. Single loss

Figure 5 shows our ionization measurements with H^+, He^+, and He^{++} at high velocities. These measurements are included for two reasons. First, they serve as a check of our apparatus since earlier measurements exist for H^+ ions (Pivovar and Levchenko[26]). Second, they illustrate the influence of projectile electrons or, in other words, the concept of effective charge (Bell *et al.*[24]).

The present results for H^+ and those of Pivovar and Levchenko[26] agree well within the combined experimental error. There seems to be a slight discrepancy for He^+ at lower energies between the present results and those of Pivovar *et al.*,[27] the origin of which is not understood. We conclude, however, that the good agreement with earlier proton data confirms the stated accuracy of our experimental procedure.

Experimental results and theory (Gillespie[22])

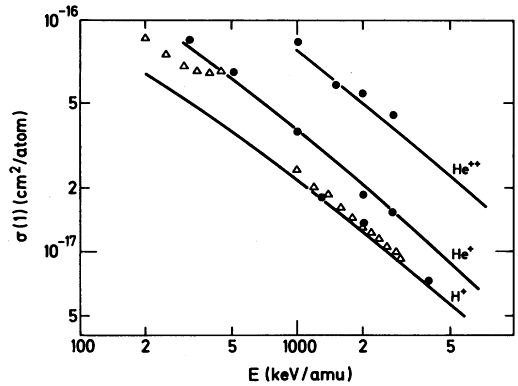

FIG. 5. Total ionization cross section of He by H^{+}, He^{+}, and He^{++}. Solid line represents the Bethe-Born calculation of Gillespie (Ref. 22). ● denotes present experimental results; Δ experimental results of Pivovar *et al.* (Ref. 27) and Pivovar and Levchenko (Ref. 26).

are in excellent agreement for all projectiles and energies. At the same time, it is confirmed that a q^2 dependence can be applied when going from H^{+} to H^{++}, while the structure of the He^{+} ion plays an important role and causes a significant variation from a q^2 scaling when He^{+} is compared with He^{++} data.

The cross sections for single loss caused by various ions of oxygen and gold incident on helium are shown in Figs. 6 and 7. From Fig. 6, where $\sigma(1)$ is plotted as a function of q, it is seen that the loss cross sections generally vary by a power of q close to one and that the cross section does not depend strongly on the type of ion. Figure 7 displays the same data, now as a function of energy per amu, and it is observed that the cross sections are nearly independent of velocity below ~100 keV/amu and decreases at higher energies. These experimental findings confirm the general picture outlined in the preceding paragraph.

Figure 8 shows the data in a reduced plot, where the single-electron-loss cross section divided by charge state is plotted versus energy in keV/amu divided by charge state. Also shown is the universal curve calculated by Olson[19] for bare nuclei as projectiles and a curve calculated by means of Eqs. (8) and (11). Taking the overall accuracy of ± 50% given by Olson[19] into account, a satisfactory agreement is obtained. However, it should be stated here that not all the measured values are expected to fall on any single curve since they correspond to interaction regimes essentially different in nature. On the other hand, more about the range of applicability of such a reduced plot can be learned by including all of the measured cross sections. Deviations from Olson's universal curve occur basically for four different reasons.

One kind of deviation is caused by the fact that

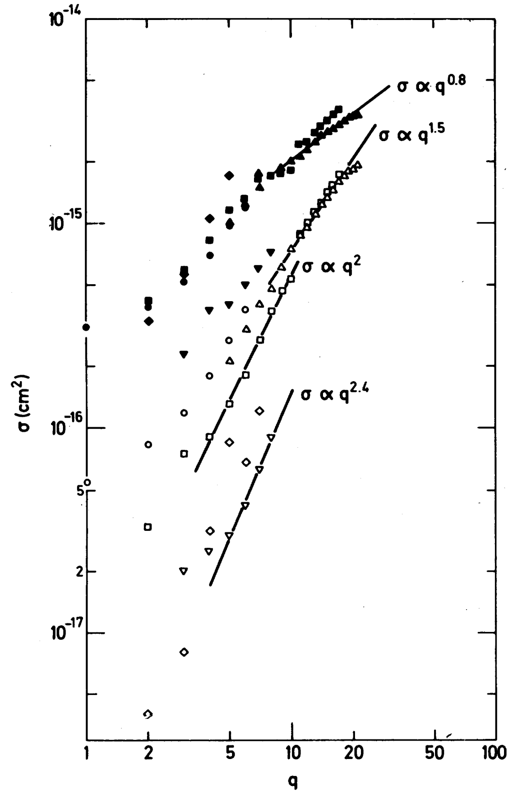

FIG. 6. Total single- (solid symbols) and double- (open symbols) loss cross sections as a function of projectile charge. ▲△ denotes 100-keV/amu Au^{q+}; ■□, 60-keV/amu Au^{q+}; ◆◇, 16.8-keV/amu Au^{q+}; ●○, 125-keV/amu O^{q+}, and ▼▽, 1-MeV/amu O^{q+}. Solid lines indicate some characteristic charge-state dependences.

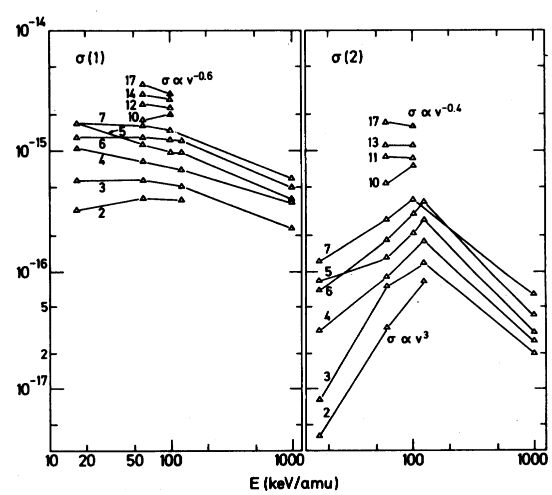

FIG. 7. Total single- $\sigma(1)$ and double- $\sigma(2)$ loss cross sections as a function of energy. Projectile charge is indicated on each curve. From left to right the points represent 16.8-keV/amu Au^{q+}, 60-keV/amu Au^{q+}, 125-keV/amu O^{q+}, and 1-MeV/amu O^{q+}.

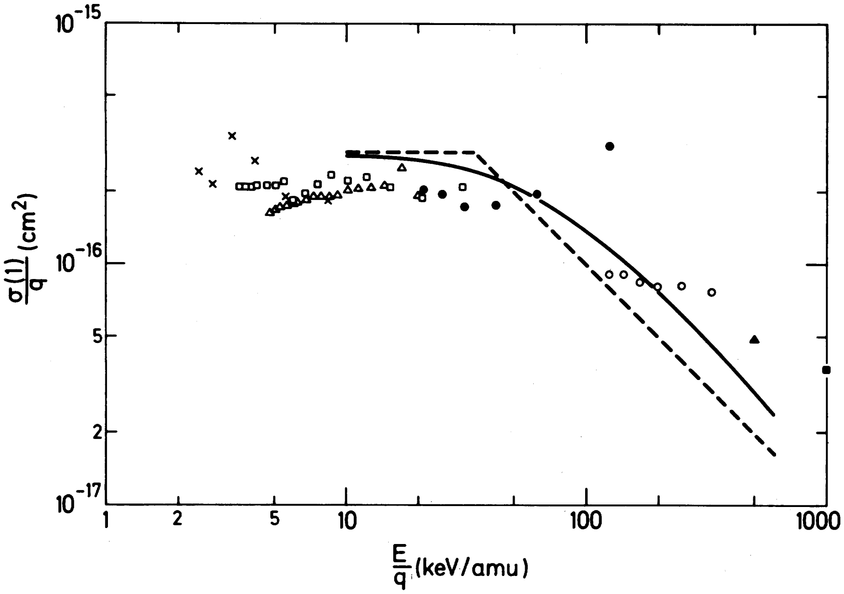

FIG. 8. Reduced plot of the single-electron cross section divided by the charge state of the incoming ion versus collision energy in keV/amu divided by charge state. Solid line represents classical-trajectory Monte Carlo calculations of Olson (Ref. 19). Dashed line is calculated from Eqs. (8) and (11) multiplied by two. Experimental results: × denotes 16.8-keV/amu Au^{q+}; □, 60-keV/amu Au^{q+}; △, 100-keV/amu Au^{q+}; ●, 125-keV/amu O^{q+}; ○, 1-MeV/amu O^{q+}; ▲, 1-Mev/amu He^{++}; ■, 1-MeV/amu He^{+}.

some of the ions used in the present measurement cannot be considered as point charges. The consequences appear for the lower charge states and are most clearly seen for O^{+} at 125 keV/amu. The measured cross sections are here considerably larger than expected for a singly charged ion, but an effective charge around 2 would bring the point down on Olson's universal curve. That the ion structure is important in this case can be understood by comparing a typical impact parameter with the radial extension of the projectile. In the present case, these are both around 0.4 Å, and a large effect from the structure is therefore not surprising. For O^{6+} at the same energy, the radial extension of the projectile is less than one tenth of a typical impact parameter for electron loss, so here the concept of a point-charge interacting with the target electrons is certainly a good approximation.

A second deviation from the general behavior is illustrated by the helium-ion points at 1 MeV/amu. The cross sections in this case are larger than the value predicted by the universal curve because quantal tunneling is neglected in the calculations (see Fig. 5). The value 500 keV/amu divided by q is stated by Olson as the upper limit of applicability of the classical Monte Carlo calculations. The unexpected charge-state dependence observed for 1-MeV/amu oxygen cross section is probably caused by a combination of the two above effects, but measurements with bare nuclei would clarify the relative importance of the two effects.

Third, the measurements for gold at 16.8 keV/amu show deviations from the general scaling rules. Such deviations might be expected when capture is the dominating electron-loss mechanism and when the charge of the projectile is low. In this case, the molecular aspects of the collision are important, but only a small number of the product channels are available. Similar deviations from scaling laws are found by, e.g., Salzborn and Müller[28] and by Bloeman *et al.*[29]

The fourth type of deviation from the universal curve is found for 100-keV/amu gold but now for the higher charge states. A decrease is here observed for the highest charge states, where double loss becomes important as a competing channel for electron loss. At $q=21$, the ratio between double loss and single loss is as large as 0.6. On the other hand, even in this case, the single-loss cross section deviates rather moderately from the general behavior, and thus this experiment supports the applicability of the exponential screening approximation used by Olson[19] to obtain an estimate of the single-electron-transition probability for a helium target.

As an example of the relative importance of the various cross sections at different velocities, the single- and double-loss and single- and double-capture cross sections (to be published) are plotted in Fig. 9 for a projectile charge of 8. Also included are measurements by Panov[30] at low energies. As far as single loss is concerned, it is evident from this plot that ionization is the dominating process at high energies, whereas capture is the dominant process at low energies.

C. Double loss

The double-loss cross sections are shown in Figs. 6 and 7. From Fig. 6 it should be noted that the variation with q is much stronger for the double-loss cross section than for the single-loss cross section. If we discuss the general behavior in terms of scaling with powers of q, it is fair to say that while the single loss varies as q, the double loss varies as q^2. A closer examination shows that for 1-MeV/amu oxygen and 16.8-keV/amu gold, the dependence is around $q^{2.5}$, while at the highest charge states for 100-keV/amu gold, the cross section is nearly proportional to q. Further, it should be noted that for any single set of measurements at fixed energy, the double-loss cross section varies with a power of q, which is almost twice the power found from the single-loss variation. By comparing the results for 125-keV/amu oxygen and 100-keV/amu gold, we observe that to a first approximation, the ions are characterized by their core charge only and not by their nuclear charge.

Figure 7 shows double-loss cross sections as a function of energy in keV/amu. We observe a maximum of the cross sections around 100-keV/amu, which corresponds to the velocity of the most firmly bound electrons in helium. On the low-energy side of this maximum, the cross section exhibits a v^3 scaling at $q=2$, but this dependence becomes weaker with increasing charge state and becomes almost independent of velocity for the highest values of q. This behavior differs from that found for single loss, where the cross section is relatively velocity independent for lower v. At high velocities, the double-loss cross section decreases with velocity as does the single-loss cross section.

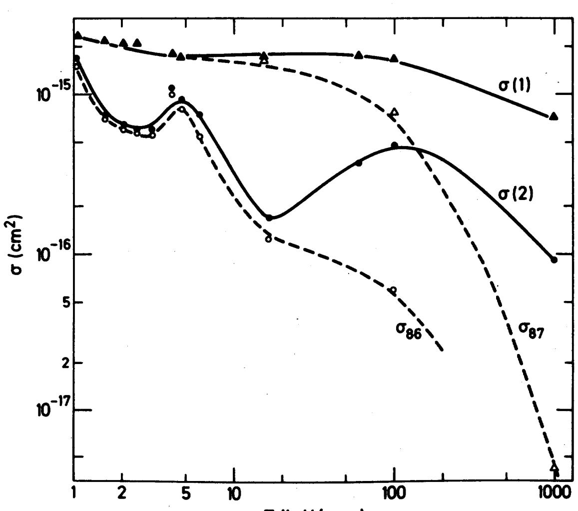

FIG. 9. Single- and double-loss and single- and double-capture cross sections for $q=8$. Results for E smaller than 10 keV/amu are for A^{8+} from Ref. 30. Results at higher energies from this paper and from forthcoming paper on electron capture.

The relative size of the two cross sections varies from 16.8-keV/amu Au^{+}, where the double-loss cross section is only 1% of the single-loss cross section, to 100-keV/amu Au^{21+}, where it amounts to 60%.

We shall now discuss some of these observations in more detail in relation to Fig. 9. As mentioned earlier, we find for single loss that at low energies, where ionization decreases with decreasing energy, electron capture becomes dominating, which results in an energy-independent cross section (see also Fig. 4 and Ref. 12). For double loss, this compensation does not occur at least for charge states smaller than 10, and accordingly a region is found where double ionization increases with increasing velocity.

The reason for the lack of capture compensation in the double-loss cross section in the region from 10 to 100 keV/amu is that double capture does not occur to a quasicontinuum of states the way single capture does but rather via Landau-Zener transitions to a small number of states. This type of collision can be understood by taking the molecular aspect of the collision into consideration, but no simple scaling rules exist in this case, as can also been seen from Fig. 9. An additional complication can arise since double capture may occur to autoionizing states followed by an Auger-autoionizing process. However, according to Kishinevskii and Parilis,[31] this process is believed to be important at somewhat lower velocities and can possibly explain the difference between double capture and double loss found by Panov[30] at low velocities.

It is found empirically that when plotting $\sigma(2)/q$ versus energy in keV/amu times q, most points fall on a universal curve within a factor of 2 (see Fig. 10). This is of course only true when plotting cross sections measured at energies smaller than ~100 keV/amu (see Figs. 6 and 7). Therefore the measurements for 1-MeV/amu oxygen are excluded from this plot. The "universal" curve can be divided into two parts, one where the cross section is proportional to q^2 times energy in keV/amu, and one where it is proportional to q but

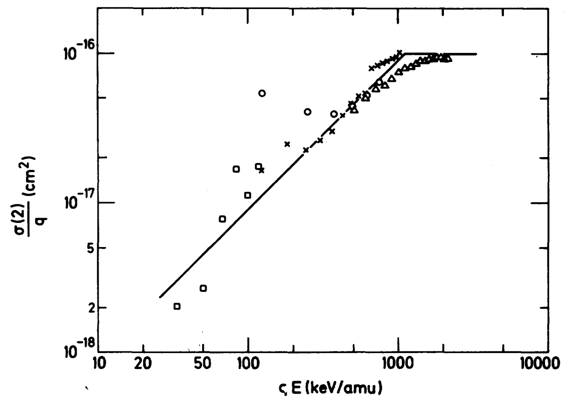

FIG. 10. Reduced plot of the double-electron-loss cross section divided by the charge state of the incoming ion versus collision energy in keV/amu divided by charge state. Solid lines represent fits to experimental results with slopes 1 and 0. Experimental results: □ denotes 16.8-keV/amu Au^{q+}; ×, 60-keV/amu Au^{q+}; △, 100-keV/amu Au^{q+}; ○, 125-keV/amu O^{q+}.

independent of energy. At present we are not aware of any simple explanation for this behavior of the double-loss cross section. Theoretical calculations by Janev and Presnyakov[11] of single ionization of atomic hydrogen by multiply charged projectiles show a nearly energy-proportional cross section below the cross-section maximum. On the other hand, the dependence on q is much weaker than that found experimentally for double loss in helium. We are well aware that this comparison should not be stretched too far, but it might give a hint as to general dependences.

At high energies, i.e., for 1-MeV/amu oxygen, the double-loss cross section can be compared with the theoretical results of Cocke[14] and Olson.[21] Figure 11 shows such a comparison. We observe good agreement with the results based on the energy-deposition model, whereas the classical Monte Carlo calculations overestimate the double-loss cross section. The same observation was found by Cocke to be generally true also for other projectile-target combinations. The single-loss cross sections are also shown in Fig. 11. For these, the theories underestimate the experimental results, once again in accordance with the findings of Cocke.

IV. SUMMARY

We have measured total single- and double-electron loss (capture plus impact ionization) by helium atoms in collisions with multiply charged ions at velocities from v_0 to $2v_0$. It is found that the cross sections for the highly charged projectiles can be characterized by the charge state

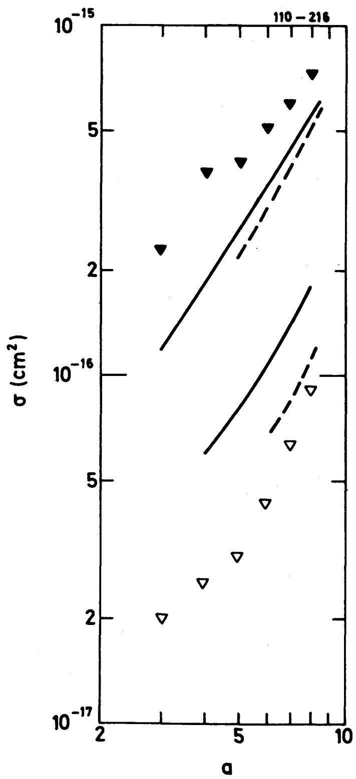

FIG. 11. Cross sections for single- and double-electron loss as a function of q for 1-MeV/amu O^{q+} ions. Solid symbols represent $\sigma(1)$ and open symbols represent $\sigma(2)$. Solid line represents classical-trajectory calculations of Olson (Ref. 21) and dashed curves represent energy-deposition calculations for 1-MeV/amu Cl ions of Cocke (Ref. 14).

only and, accordingly, do not depend on the atomic number of the ion. For lower charge states, a deviation from this point-charge description is observed.

The single-loss cross sections can most conveniently be presented in a reduced plot, where cross section divided by charge state is plotted versus energy per mass unit divided by charge state. The measurements confirm the theoretical calculations of Olson[19] for a helium target the same way the Berkeley measurements[20] confirmed similar calculations for a hydrogen target.

The single-loss cross section is almost independent of energy at low (less than 100 keV/amu) energies. This is in strong contrast to the behavior found for double loss, where the cross section is almost proportional to energy in the same energy region. It is suggested that the different energy behavior in the two cases can be explained by a strong change in the relative importance of electron capture, i.e., double-electron capture is relatively unimportant at velocities from v_0 to $2v_0$.

[1]H. B. Gilbody, in *Advances in Atomic and Molecular Physics*, edited by D. R. Bates and B. Bedersen (Academic, New York, 1979), Vol. XV, p. 293.
[2]F. J. de Heer, in *NATO Advanced Study Institute on Atomic and Molecular Processes in Controlled Thermonuclear Fusion*, edited by M. R. C. McDowell and A. M. Ferendeci (Plenum, New York, 1980), p. 351.
[3]R. E. Olson, in *Book of Invited Papers of the XI ICPEAC, Kyoto, 1979*, edited by N. Oda and K. Takayanagi (North-Holland, Amsterdam, 1980), p. 391.
[4]E. Salzborn and A. Müller, in *Book of Invited Papers of the XI ICPEAC, Kyoto, 1979*, edited by N. Oda and K. Takayanagi (North-Holland, Amsterdam, 1980), p. 407.
[5]N. Bohr, K. Dan. Vidensk. Selsk. Mat. Fys. Medd. 18, No. 8 (1948).
[6]G. I. Bell, Phys. Rev. 90, 548 (1953).
[7]N. Bohr and J. Lindhard, K. Dan. Vidensk. Selsk. Mat. Fys. Medd. 28, No. 7 (1954).
[8]N. O. Lassen, K. Dan. Vidensk. Selsk. Mat. Fys. Medd. 26, No. 5 (1951); 26, No. 12 (1951).
[9]H. D. Betz, Rev. Mod. Phys. 44, 465 (1972).
[10]E. L. Duman, L. I. Men'shikov, and B. M. Smirnov, Zh. Eksp. Teor. Fiz. 76, 516 (1979) [Sov. Phys.—JETP 49, 260 (1979)].
[11]R. K. Janev and L. P. Presnyakov, Phys. Rev. A (in press).
[12]R. E. Olson and A. Salop, Phys. Rev. A 16, 531 (1977).
[13]H. Ryufuku and T. Watanabe, Phys. Rev. A 20, 1828 (1979).
[14]C. L. Cocke, Phys. Rev. A 20, 749 (1979).
[15]M. Kaminsky, in *Atomic and Ionic Impact Phenomena on Metal Surfaces* (Springer, Berlin, 1965), p. 276.
[16]H. S. W. Massey and H. B. Gilbody, in *Electronic and Ionic Impact Phenomena* (Clarendon, Oxford, 1974), Vol. IV, p. 2556.
[17]C. N. Burrous, A. J. Lieber, and V. T. Zaviantseff, Rev. Sci. Instrum. 38, 1477 (1967).
[18]J. J. Thomson, Philos. Mag. 23, 449 (1912).
[19]R. E. Olson, Phys. Rev. A 18, 2464 (1978).
[20]R. E. Olson, K. H. Berkner, W. G. Graham, R. V. Pyle, A. S. Schlachter, and J. W. Stearns, Phys. Rev. Lett. 41, 163 (1978).
[21]R. E. Olson, J. Phys. B 12, 1843 (1979).
[22]G. H. Gillespie, Phys. Lett. 72A, 329 (1979).
[23]M. Inokuti and Y.-K. Kim, Phys. Rev. 186, 100 (1969).
[24]K. L. Bell, V. Dose, and A. E. Kingston, J. Phys. B 3, 129 (1970).
[25]K. L. Bell and A. E. Kingston, J. Phys. B 2, 653 (1969).
[26]L. I. Pivovar and Yu. Z. Levchenko, Zh. Eksp. Teor. Fiz. 52, 42 (1967) [Sov. Phys.—JETP 25, 27 (1967)].
[27]L. I. Pivovar, Yu. Z. Levchenko, and A. N. Grigor'ev, Zh. Eksp. Teor. Fiz. 54, 1310 (1968) [Sov. Phys.—JETP 27, 699 (1968)].
[28]A. Müller and E. Salzborn, Inst. Phys. Conf. Ser. 38, 169 (1978).
[29]E. Bloemen, H. Winter, F. J. de Heer, R. Fortner, and A. Salop, J. Phys. B 11, 4207 (1978).
[30]M. N. Panov, in *Book of Invited Papers XI ICPEAC, Kyoto, 1979*, edited by N. Oda and K. Takayanagi (North-Holland, Amsterdam, 1980), p. 437.
[31]L. M. Kishinevskii and E. S. Parilis, Zh. Eksp. Teor. Fiz. 55, 1932 (1968) [Sov. Phys.—JETP 28, 1020 (1969)].